# Accuracy Assessment of Burned Area Products in the Orinoco Basin

**Jesús A. Anaya and Emilio Chuvieco**

## Abstract

*Appropriate assessment of the accuracy of burned area products is required to assess greenhouse gas (GHG) emissions in a reliable way. This paper provides validation results for three burned area products with different pixel sizes: MCD45 (500 m), GlobCarbon (1 km), and L3JRC (1 km) for the Orinoco River basin, which is widely affected by fires, many of them oriented towards the conversion of Amazonian forest to cattle pasture. Accuracy measurements were based on commission and omission errors computed from 15 confusion matrices, as well as in the Pareto Boundary concept, which evaluates the impact of different pixel sizes in omission and commission errors. An edge metric was used to analyze the impact of shapes of burned patches on global accuracy. It was shown that all products underestimate burned-area and that an increase in pixel size or burned patch elongation, results in larger estimation errors.*

## Introduction

Biomass burning creates a large variety of impacts on a local, regional, and global scale. Even though fire has been recognized as a natural process in various ecosystems, it has also been associated with negative effects on soil, water, vegetation, and the atmosphere. At a local scale, it has been found that fire impacts soil erosion (Shakesby *et al.*, 2007) and alters vegetation succession (Clemente *et al.*, 2006). At a regional scale there is a need for nations to meet the Kyoto protocol, to achieve sustainability of forest ecosystems, and to reduce large biomass burning emissions. Finally, at a global scale there is a growing concern regarding biomass burning in relation to global warming, greenhouse gas (GHG) emissions and changes in the properties and composition of the atmosphere (Chuvieco, 2008). Seiler and Crutzen (1980) proposed a bottom-up method to estimate biomass emissions based on the variables involved in the process: Areas burned (vegetation affected by fire), biomass load (carbon available for combustion), burning efficiency (fraction of biomass consumed by the fire), and emission factors (amount of each substance emitted per unit of carbon burned). There are different levels of uncertainty in each of these variables, which in turn result in emissions uncertainties.

Tropical forests are large carbon pools at regional and global levels. However, today these forests are undergoing deforestation at unprecedented rates (Achard *et al.*, 2002), releasing carbon dioxide and contributing to the global greenhouse effect (Fearnside, 2000a). Fire is commonly used in the tropics as a tool for deforestation and forest degradation, associated with agricultural activities and cattle grazing (Fearnside, 2000b). Biomass burning is induced during the dry season, and its negative effects are worsened with natural phenomena like the El Niño Southern Oscillation (ENSO) (Levine *et al.*, 1999). A detailed description of biomass burning in the tropics and specific emission factors for these regions can be found in Levine (2000).

Remote sensing techniques are used to monitor active fires and estimate the extent of burned areas (Chuvieco, 2008). Active fires are detected by the thermal contrast between burning pixels and surrounding areas, while burned areas are commonly discriminated from the strong reflectance change between pre- and post-fire images. This signal is less evident than the thermal contrast of active burning, but it last longer. In any case, the actual magnitude of post-fire reflectance depends on fire characteristics and ecosystem resilience after fire. Therefore, considerable uncertainties remain in the mapping of burned areas, particularly in the tropics where burnings are done usually in small patches ($<1$ km$^2$) (Schultz *et al.*, 2008). Developing international networks to validate burned areas estimations is required to increase quality and economize validations (Roy and Boschetti, 2009b). This paper focuses on the validation of burned area estimation, known as burned area (BA) products, in the tropical savannas of the Orinoco Basin.

Several projects have been carried out to map burned areas at global scale. In the year 2000, two global BA products were developed. They were known as GBA2000 -Global Burnt Areas- (Tansey *et al.*, 2004) and GlobScar (Simon *et al.*, 2004). The former was based on SPOT VEGETATION (VGT) images and the latter on ERS Along Track Scanning Radiometer (ATSR) instrument data. The goal of these two products was to create homogeneous information at a global scale with a standard methodology (Hoelzemann *et al.*, 2004). From the experience of GBA2000, a longer time series was generated based on SPOT-VEGETATION images as well. The final product was named L3JRC. Similarly, following the experience of Globscar, the European Space Agency (ESA) developed the GlobCarbon project, which combines SPOT VGT and ATSR images. More recently, a BA product based on the Moderate Resolution Imaging Spectroradiometer (MODIS) data have been made available (named MCD45).

Burned area products include uncertainties and errors due to several factors. First, the spatial resolution of the input sensor prevents discriminating small burn patches (especially in fragmented landscapes) (Smith *et al.*, 2003; Silva *et al.*, 2005a). Second, an important source of error is the spectral overlapping between BA and non-vegetated covers (dark soils, shadows, water bodies), which makes

Jesús A. Anaya is with the Universidad de Medellín, Carrera 87 No.30-65, Medellín, Colombia, S.A (janaya@udem.edu.co).

Emilio Chuvieco is with the Universidad de Alcalá, Calle Colegios 2, 28801, Alcalá de Henares, Madrid, España.

Photogrammetric Engineering & Remote Sensing
Vol. 78, No. 1, January 2012, pp. 53–60.

0099-1112/12/7801–53/$3.00/0

more difficult the singular characterization of burned patches. Atmospheric influences, such as clouds or smoke plumes, preset challenges to burned land discrimination as well, particularly in cloudy tropical regions. Finally, the burned signal is not unique, but rather is affected by several factors that introduce wide reflectance variation, such as the type of burned coverage, combustion completeness, fraction of material exposed to the fire, and post fire physical evolution of the surface (Ward *et al.*, 1996; Miller and Yool, 2002; Roy and Landmann, 2005).

The objective of this study was to assess the quality of three available global BA products in the savanna ecosystem of the Orinoco Basin by comparing them to the BA interpretation of high resolution satellite images. The most relevant accuracy components are the omission of burned areas and the assignment of burned areas to areas that are not burned. Another component of concern is the poor spatial resolution (mixed pixels) associated to global products.

## Methods

The study area is located in the northern savannas of South America along the tributaries of the Orinoco River (Figure 1) with an area of approximately one million square kilometers. The area is highly prone to fires due to pasture burning and forest clearing. In fact, Colombia and Venezuela have been found to be among the most affected countries in Latin America by biomass burning (Chuvieco *et al.*, 2008). Increasing deforestation in the Amazon rainforest due to the growing need of lands for cropping and grazing has created a broad mosaic of burned areas. Temporal priority was given to the dry season months of January, February, and March.

The confusion matrix method has been commonly used since the 1980 to validate thematic maps (Congalton, 2001) including BA products (Roy *et al.*, 2005a; Boschetti *et al.*, 2006b; Boschetti *et al.*, 2009; Roy and Boschetti, 2009a). The confusion matrix is used to calculate the accuracy of thematic maps by comparing classified maps with reference information. Reference information is usually located in the columns of the matrix, and the thematic map is located in the rows. Diagonal values indicate correctly classified data, while the rest of the cells indicate either omission or commission errors.

### Burned Area Products Included in the Assessment

Three BA products were validated (Table 1):

1. L3JRC is based on the VEGETATION instrument onboard the SPOT-4 and -5 satellite (Tansey *et al.*, 2007) with a 1 km spatial resolution and daily global acquisition. The BA detection algorithm was developed by the International Forest Institute (IFI) and uses a temporal index based on the near infrared (NIR) band. This database is provided on an annual basis, assuming that an area may burn only once in a fire year.
2. GlobCarbon is the continuation of the GlobScar project that started in 2001, with data from the ATSR on board ERS-1, ERS-2, and more recently on the Envisat European satellites (Simon *et al.*, 2004). The input images have 1 km spatial resolution and are acquired globally every other day. The basic BA algorithms were developed by IFI and by the Technical University of Lisbon (UTL). Therefore, GlobCarbon includes more detection algorithms than L3JRC and data from both SPOT VEGETATION and ATSR. The database is provided on a monthly basis and includes the date of detection and the algorithm used to detect BA.
3. MCD45 is the official MODIS BA product (Silva *et al.*, 2005b). This product has a 500 m spatial resolution and detects burned-areas based on a predicted reflectance. The algorithm evaluates whether the predicted reflectance (based on the bidirectional reflectance distribution function) and observed reflectance indicate significant change. Each burned pixel provides an eight-day temporal precision due to missing observations. Despite all these products (Table 1) depicting fire occurrence every day of the year, data is provided to users as monthly or as annual files.

### Reference Data

The validation process requires comparing an assessed product with an independent dataset, which is assumed to be ground truth. Since it is very difficult to obtain such accurate reference information by field work, a common proxy to generate reference data is the interpretation of high

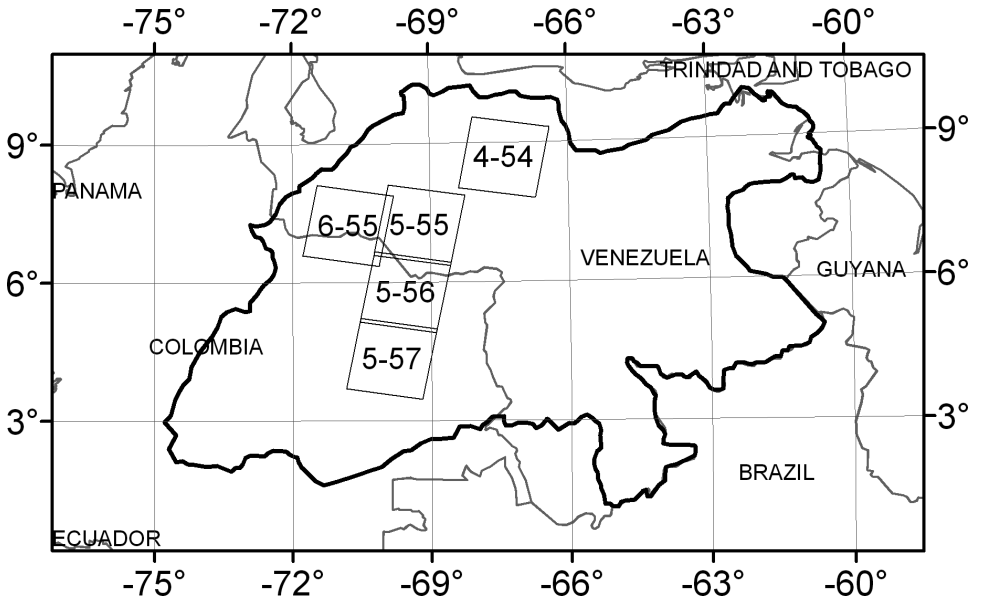


Figure 1. Orinoco basin and (Path / Row) location of the Landsat images used for validation in the areas with largest biomass burning in Colombia and Venezuela.

TABLE 1. GLOBAL BURNED-AREA PRODUCTS INCLUDED IN THE VALIDATION EXERCISE

| | Spatial resolution (m) | Temporal availability | Product availability | Projection | Citation |
|---|---|---|---|---|---|
| L3JRC[1] | 1,000 | Annual | 2000-2007 | PlateCarrée | (Tansey *et al.*, 2007) |
| MCD45[2] | 500 | Monthly | 2000-Today | Sinusoidal | (Roy *et al.*, 2005b) |
| GlobCarbon[3] | 1,000 | Monthly | 1998-2007 | PlateCarrée | (Simon *et al.*, 2004) |

[1] http://bioval.jrc.ec.europa.eu/
[2] https://wist.echo.nasa.gov/
[3] http://www.geosuccess.net/

resolution satellite images. On one hand, it is almost impossible to cover the geographic extent of a regional or global product with field work. On the other hand, the post-fire signals last shortly, and ground information has to be restricted to few plots. Therefore, higher resolution images acquired at the same time as the coarse resolution that are to be evaluated is the only operational means to generate reference fire perimeters (Boschetti *et al.*, 2006a). Landsat images have been successfully used in previous studies as a proxy for field work because they have an adequate spatial, temporal and spectral level of detail to identify and delimit burned patches (Roy *et al.*, 2005b; Boschetti *et al.*, 2006a; Chuvieco *et al.*, 2008). The only available protocol for this type of validation uses this approach (Roy *et al.*, 2005).

Five pairs of Landsat ETM+ (**www.landcover.org**) images were visually interpreted based on a multitemporal visual comparison protocol (Roy *et al.*, 2005). BA polygons were interpreted using pairs within a time range of maximum three months (first and second acquisition) and with the same location or World Reference System (WRS) (Table 2), interpretation requires to overlay each pair of images in order to identify and polygon digitize a burned patch in the second acquisition date that did not exist in the first acquisition date. This allows determining the time frame of fire occurrence required to validate BA products. Reference images were selected based on low cloud cover content and evidence of BA. Selecting reference images through a statistical design would have been impossible following these constraints, since the area is highly cloudy. The geographic extension of the selected scenes corresponds to 16.5 percent of the study area, which includes savanna, primary forest, and secondary forest.

### Processing and Validation of Global BA Products

The BA products were reprojected to UTM19-WGS84 in order to use the same projection as the reference data. No evidence of location errors were found when overlaying reference polygons on BA products. Only those pixels burned between the first and second Landsat acquisition dates were taken into account for the validation. Common areas between the reference and the global BA product were extracted and resampled to 30 m $\times$ 30 m pixel size. Consequently, the same areas and pixel sizes were considered in both reference and global product. A confusion matrix was calculated for each Landsat scene and all the pixels were used to calculate global accuracy and Kappa coefficient. Global and Kappa statistics are commonly reported with the confusion matrix, global accuracy is the sum of the diagonal values divided by the total number of pixels. Kappa evaluates the level of agreement that can be expected due to chance alone (Hudson and Ramn, 1987; Congalton and Green, 1999). A value of 1 implies a perfect agreement and 0.5 a fair agreement. If negative, the estimation result is worse than that expected by chance.

$$\text{Global accuracy} = \frac{\sum_{i=1}^{k} n_{ii}}{n} \tag{1}$$

$$\text{and Kappa coefficient} = \frac{n\sum_{i=1}^{k} n_{ii} - \sum_{i=1}^{k} n_{i+}n_{+j}}{n^2 - \sum_{i=1}^{k} n_{i+}n_{+j}} \tag{2}$$

where, $n$ is total number of validation pixels, $n_{ii}$ is the diagonal agreements, $n_{ij}$ is the number of pixels classified into category $i$ ($i$ = burned, non-burned) in the map and category $j$ ($j$ = burned, non-burned) in the reference data, $n_{i+}$ is the sum of $n_{ij}$ in the BA product (rows), and $n_{+j}$ is the sum of $n_{ij}$ in the reference BA (columns)

Omission errors (OE) were calculated as the ratio of false negatives to the total number of pixels in the reference BA. Commission errors (CE) were calculated as the ratio of the false positives to the total number of pixels in the ba global product.

Additionally, the Pareto Boundary (PB) described by Boschetti *et al.* (2004b) was calculated in order to determine the effect of various pixel sizes (500 m for MCD45 and 1 km for L3JRC and GlobCarbon) on map accuracy. The PB was defined as a set of points that belong to the boundary and drawn in a two dimension (OE/CE) coordinate system. To calculate each point, a low resolution grid with a cell size of 500 m or 1 km had to be overlaid on the high resolution image (reference), so that the proportion of BA of each cell overlaying this image could be computed (Figure 2). If only those cells which are 100 percent burned on the low resolution map are considered as burned, the commission error is zero but the omission error is extremely high. If on the other hand, a cell is considered as burned with any percentage of BA, the omission error (OE) is zero, but the commission error

TABLE 2. STATISTICS OF BURNED AREAS BASED ON LANDSAT ETM+ IMAGES

| | First acquisition | Second acquisition | Number of burn polygons | Burned area (km$^2$) | Burned[a] Area (%) |
|---|---|---|---|---|---|
| ETM+P004R054 | 12302002 | 01312003 | 3,733 | 2,891 | 8.4 |
| ETM+P005R055 | 01032002 | 02202002 | 7,914 | 4,148 | 12.2 |
| ETM+P005R056 | 01062003 | 01222003 | 1,937 | 2,168 | 6.3 |
| ETM+P005R057 | 01062003 | 01222003 | 2,982 | 1,958 | 5.7 |
| ETM+P006R055 | 01232001 | 02242001 | 1,881 | 933 | 2.7 |

[a] The area of a Landsat-ETM+ image is approximately 32,400 km$^2$

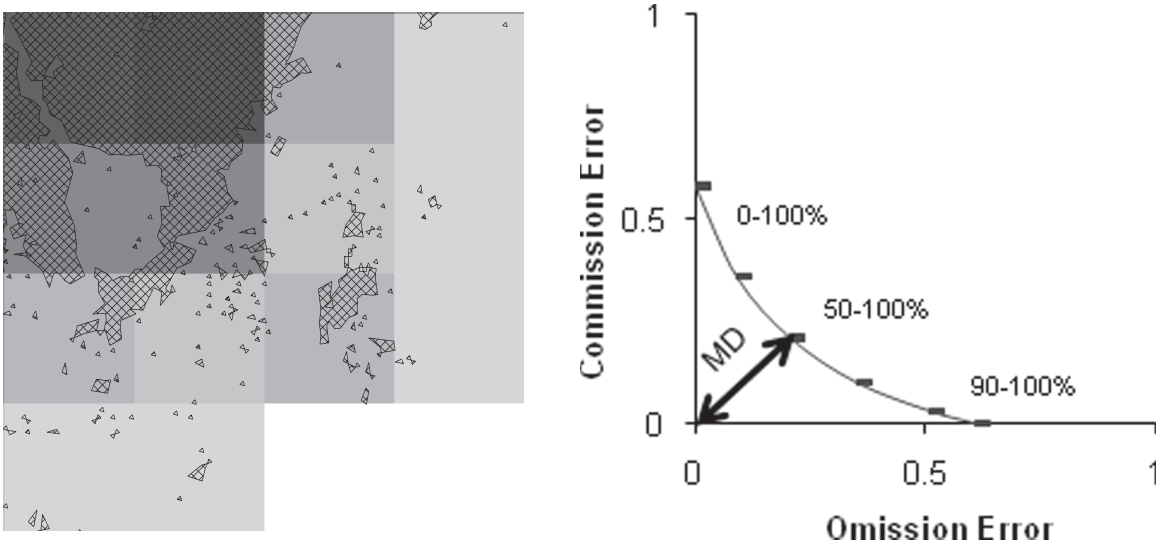


Figure 2. (a) Subset of a low resolution grid overlaid on a high-resolution image and the Pareto Boundary. The percentage of burned-area on the low resolution cells changes from non-burned cells (white, 0 percent) to completely burned cells (black, 100 percent). (b) The selection of thresholds (*t*) results in coordinate pairs of Omission and Commission errors (OE/CE). The MD arrow represents the minimum distance from the CE/OE origin to the Pareto Boundary. The distance from the origin (no commission or omission errors) to the PB is a measure of the inaccuracy due to pixel size for a given Landsat scene.

(CE) is extremely high. Intermediate points were calculated at different percentages of BA on the low resolution map in order to get more (OE/CE) coordinates. In other words, the set of coordinates (OE/CE) belonging to the PB was created by changing the percentage threshold (*t*) in which a cell would be considered as burned. Five thresholds (90 to 100 percent, 75 to 100 percent, 50 to 100 percent, 25 to 100 percent, 0 to 100 percent) were used for each pair of reference image and low resolution maps to describe the PB.

The PB evaluates the effect of low resolution products on BA boundaries and small burned fragments. This curve defines the trade-off between omission and commission errors when a partially burned pixel is classified as a burned or unburned pixel. For this reason, this method does not consider commission errors due to dark surfaces (e.g., shadow or dark soils) or under detection due to low reflectance differences before and after the fire.

In addition to the PB, which mainly describes the best possible combination of OE and CE due to the effect of pixel size, a landscape metric known as edge density (ED) was calculated to describe the effect of fragmentation. This metric is based on the area and perimeter of burned-are (Fassnacht *et al.*, 2006; Miettinen, 2007), and it is a measure of the complexity and shape of the polygons. ED was calculated as:

$$ED = \sum(P_m)/\sum(A_m) \quad (3)$$

where, ED (m/ha) is the Edge Density, P (m) is the Perimeter for each *m* BA patch, and A (ha) is the Surface area for each *m* BA patch.

Large values of Edge Density indicate complex shapes and long borders, while low values indicate simple and compact shapes (Silva *et al.*, 2005a). This metric was calculated for each reference scene to evaluate the effect of fragmentation on the PB. Seven additional Landsat images (single date) were processed in order to increase the sample size and adjust a linear regression of ED against MD.

## Results

The results of the 15 confusion matrices calculated from the reference images and each of the products evaluated are shown in Table 3. In general, global accuracy is close to

TABLE 3. PAIRS OF COORDINATES OE/CE FOR BURNED-AREA OF A TOTAL OF 15 CONFUSION MATRICES; MEAN VALUES OF ACCURACY MEASUREMENTS ARE SHOWN IN BOLD

| First acquisition date | Omission error | Commission Error | Global accuracy (%) | Kappa coefficient |
|---|---|---|---|---|
| | | MCD45 | | |
| 12302002 | 50.03 | 34.80 | 95.84 | 0.54 |
| 01032002 | 80.50 | 35.70 | 92.83 | 0.27 |
| 01062003 | 31.31 | 32.12 | 97.33 | 0.66 |
| 01062003 | 43.17 | 29.75 | 97.36 | 0.61 |
| 01232001 | 76.35 | 48.34 | 98.29 | 0.31 |
| **Mean** | **56.27** | **36.14** | **96.33** | **0.48** |
| | | L3JRC | | |
| 12302002 | 77.55 | 45.84 | 94.06 | 0.29 |
| 01032002 | 82.81 | 42.82 | 91.73 | 0.24 |
| 01062003 | 64.67 | 48.87 | 95.53 | 0.39 |
| 01062003 | 81.74 | 47.09 | 95.91 | 0.25 |
| 01232001 | 86.48 | 60.78 | 97.95 | 0.19 |
| **Mean** | **78.65** | **49.08** | **95.04** | **0.27** |
| | | GlobCarbon | | |
| 12302002 | 63.21 | 58.44 | 90.02 | 0.33 |
| 01032002 | 60.42 | 50.94 | 93.44 | 0.40 |
| 01062003 | 45.37 | 50.57 | 95.39 | 0.49 |
| 01062003 | 62.43 | 45.96 | 96.06 | 0.42 |
| 01232001 | 78.24 | 59.59 | 97.89 | 0.27 |
| **Mean** | **61.93** | **53.10** | **94.56** | **0.38** |

90 percent due to the large number of the unburned category agreements, and therefore, not a good measurement to assess the accuracy of BA, but when considering the Kappa coefficient, the agreement decreases. Omission errors for BA tend to be higher than commission errors, with omitted values larger than 50 percent of burned category, which leads to an underestimation of total BA. When comparing the three global products the best accuracy measurements were found for MCD45. This product has the lowest commission and omission errors and the highest global accuracy and Kappa coefficients (Table 3). The results from GlobCarbon and L3JRC, both with 1 km spatial resolution, were similar. Only omission errors and Kappa measurements are statistically different (t-test), where GlobCarbon has a lower omission error (P-value: 0.002) and a higher Kappa value (P-value: 0.01).

Although there is a tendency towards larger omission errors (Figure 3) there is also a large dispersion of OE/CE values. Dispersion is reduced drastically when OE/CE values are considered by Landsat scenes, i.e., algorithms behave similarly within scenes but are highly variable among scenes.

In order to find the reliability of the BA product algorithms and to assess the effect of pixel size, the PB method was applied. The area under the PB curve is defined by Boschetti (2004) as the unreachable region, there is no combination of OE/CE values for a given pixel size that could result in values under this curve. Thus, the OE/CE values from the confusion matrix are above the PB and their distances represent the potential of the BA algorithm to be improved. The PB was calculated for the reference images and each combination of reference images with a low resolution grid results in a different boundary. It was found that the area under the PB is always lower for a 500 m pixel than for a 1 km pixel. However, the distance from the OE/CE points to the PB curve, calculated with the same resolution grid, varies. The closest distance between OE/CE values and its corresponding PB was measured in order to compare the three global products. OE/CE values far from the PB indicate poor performance, in contrast, the pairs of OE/CE values closer to its PB, indicate better quality of the algorithm. The mean distance value for the five Landsat scenes was 0.25 for MCD45, 0.28 for GlobCarbon, and 0.35 for L3JRC. These values indicate the inaccuracy due to the algorithms disregarding pixel size (Figure 4).

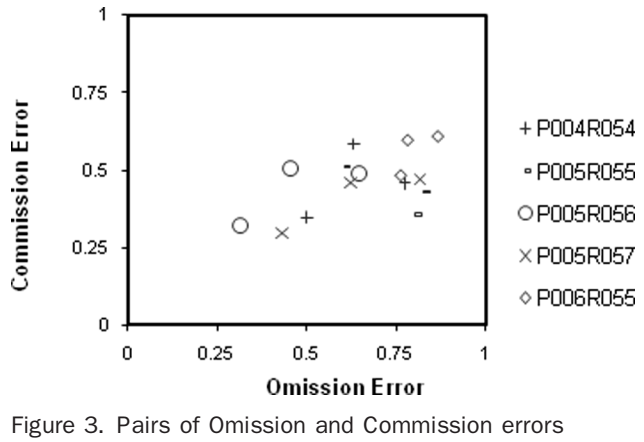


Figure 3. Pairs of Omission and Commission errors calculated using a confusion matrix; the same symbol is used for the three global products in each Landsat scene.

Since the PB is sensitive to the size of the pixels, it should also be affected by the landscape distribution of the BA fragments. ED was calculated per scene using area and perimeter of BA fragments in an unburned matrix; note that global BA products are not included in this process. Twelve PB curves, one for each landscape were calculated with a grid of 1 km. Figure 5 relates PB to their respective edge density (ED) metrics. An increase in the ED metric corresponds to larger areas under the PB, i.e., larger inaccuracies. The minimum distance from the origin to the PB (MD) was used as an index of BA global product inaccuracy due to pixel size. When relating this index to ED a strong linear relationship was found ($R^2 = 0.89$) as shown in Equation 4:

$$MD = 0.0045\,ED + 0.1718 \quad (4)$$

where, MD is the minimum distance from origin to PB, and ED (m/ha) is the Edge Density

## Discussion and Conclusions

A major challenge when validating BA products is to achieve the largest possible temporal coherence between the date of the high-resolution reference images and the product to be validated. This is only possible if both data sources (Landsat and global products) show the day of detection for each burned pixel. For this reason it was necessary to obtain two Landsat images of the same fire season as close in time as possible. Since MODIS BA provided eight-day precision due to the occurrence of missing information, burned areas detected by the algorithm after the second Landsat acquisition were quantified as omissions.

As discussed above, validation was made depending on the BA product and the reference image availability. It was found that L3JRC and GlobCarbon presented similar commission errors (49 percent and 53 percent, respectively), but omission errors were lower in GlobCarbon (62 percent) than in L3JRC (79 percent). MCD45 had the lowest omission and commission errors, 56 percent and 36 percent, respectively. These results indicate that the best BA product is MCD45. No false detections were found with dark soils or cloud shadow. A visual inspection of the commission errors in the high resolution images showed that most of these errors are associated with mixed pixels (i.e., pixels along the boundaries of burned-areas) or adjacent burned fragments that are merged into one larger fragment.

In the study area it was found that omission errors were larger than commission errors for all the evaluated products. This is similar to what has been observed by other authors in the savannas of northern South America (Romero-Ruiz *et al.*, 2010) and Africa (Barbosa *et al.*, 1999; Silva *et al.*, 2005b; Roy and Boschetti, 2009b). In terms of estimation GHG derived from biomass burning, our results show a tendency to underestimate GHG emissions using these global products. The under detection of burned-areas is most significant when fire affects forested areas, particularly in small patches. This may greatly impact GHG estimations, since these small fires are occurring at a vegetation class with large biomass values >300 Mg $ha^{-1}$ (Anaya *et al.*, 2009).

The PB has been shown to be sensitive to both pixel size and the BA distribution in the landscape. The Edge Density landscape metric is easy to calculate, and its simplicity allows for a straightforward interpretation. Here, it was shown that increases in pixel size as well as in fragmentation of burned-areas result in larger omission and commission errors. In contrast, the distance between the OE/CE values with their respective PB is quite similar among global BA products. This shows that the size of the pixel of the BA product is more important than differences between

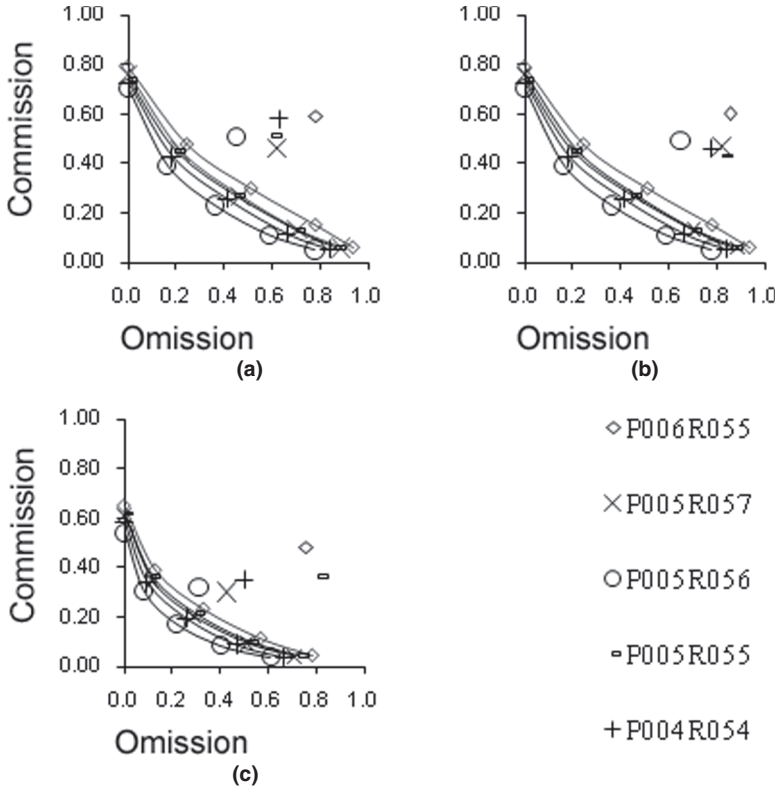


Figure 4. Pareto Boundary and confusion matrix commission and omission errors for the three BA products: (a) GlobCarbon (1 km), (b) L3JRC (1 km), and (c) MCD45 (500 m). This figure provides an understanding of whether the confusion matrix OE/CE values could be reduced by improving the algorithm, or if the error is only related to the low spatial resolution of the product.

algorithms, for this reason new BA products should be based on higher spatial resolution images.

When estimating burned-areas or (GHG) carbon emissions, Hoelzemann (2004) and Roy (2005b) concluded that different satellite information should be considered. In this sense, and as an alternative to minimize omission errors in forests, several authors (Boschetti *et al.*, 2004a; Giglio *et al.*, 2009) have found that active fire information may very useful for burned land mapping. In terms of area estimation of actual burnings, commission errors can partially compensate those from omissions, but the precise mapping of BA is very critical to improve GHG emissions since the pre-fire biomass loads plays a critical role in the amount of gas released as a result of fire (Ward *et al.*, 1996).

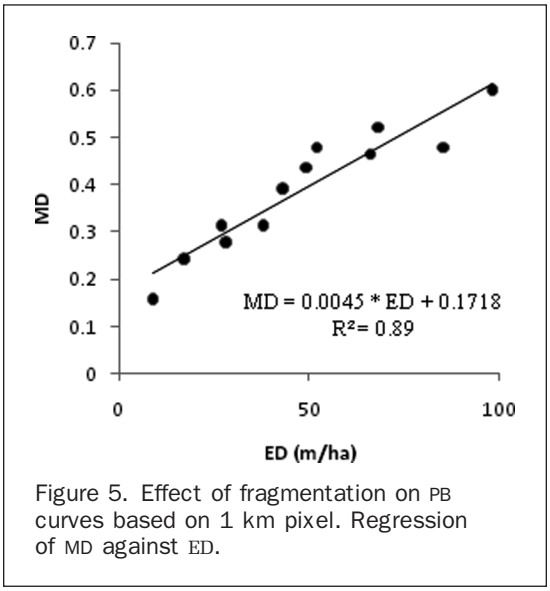


Figure 5. Effect of fragmentation on PB curves based on 1 km pixel. Regression of MD against ED.

## Acknowledgments

This study was supported by The Universidad de Medellín - Colombia (7000001823) and the European Commission program AlBan (E05D059391CO). The authors would like to thank the Latin American Remote Sensing and Forest Fires Network (RedLaTIF) for their comments and suggestions, and are grateful to Mr. Sebastian Palomino for his expertise and support in image interpretation.

## References

Achard, F., H. Eva, H.-J. Stibig, P. Mayaux, J. Gallego, T. Richards, and J.-P. Malingreau, 2002. Determination of deforestation rates of the world's humid tropical forests, *Science*, 297(9):999–1002.

Anaya, J.A., E. Chuvieco, and A. Palacios-Orueta, 2009. Above-ground biomass assessment in Colombia: A remote sensing approach, *Forest Ecology and Management,* 257(4):1237–1246.

Barbosa, P.M., D. Stroppiana, J.M. Gregoire, and J.M.C. Pereira, 1999. An assessment of vegetation fire in Africa (1981-1991): Burned areas, burned biomass and atmospheric emissions, *Global Biogeochemical Cycles*, 13:933–950.

Boschetti, L., P.A. Brivio, H. Eva, J. Gallego, A. Baraldi, and J.M. Gregoire, 2006a. A sampling method for the restrospective validation of global burned area products, *IEEE Transactions on Geoscience and Remote Sensing,* 44:1765–1772.

Boschetti, L., P.A. Brivio, H.D. Eva, J. Gallego, A. Baraldi, and J.M. Gregoire, 2006b. A sampling method for the retrospective validation of Global Burned Area products, *IEEE Transactions on Geoscience and Remote Sensing*, 44(7):1765–1773.

Boschetti, L., H.D. Eva, P.A. Brivio, and J.M. Gregoire, 2004a. Lessons to be learned from the comparison of three satellite-derived biomass burning products, *Geophysical Research Letters*, 31(L21501):doi:10.1029/2004GL021229.

Boschetti, L., S.P. Flasse, and P.A. Brivio, 2004b. Analysis of the conflict between omission and commission in low spatial resolution dichotomic thematic products: The Pareto Boundary, *Remote Sensing of Environment*, 91(3-4):280–292.

Boschetti, L., D.P. Roy, and C.O. Justice, 2009. International Global Burned Area Satellite Product Validation Protocol, Part I – Production and standardization of validation reference data, URL: *http://lpvs.gsfc.nasa.gov/DOC/protocol_revised_Apr09.doc* (last date accessed: 03 October 2011).

Clemente, R.H., R.M.N. Cerrillo, J.E.H. Bermejo, and I.Z. Gitas, 2006. Modelling and monitoring post-fire vegetation recovery and diversity dynamics: A diachronic approach using satellite time-series data set, *Forest Ecology and Management,* 234(Supplement 1):S194–S194.

Congalton, R.G., 2001. Accuray assessment and validation of remotely sensed and other spatial information, *International Journal of Wildland Fire*, 10:321–328.

Congalton, R.G., and K. Green, 1999. *Assessing the Accuracy of Remotely Sensed Data: Principles and Applications*, Lewis Publishers, Boca Raton, Florida.

Chuvieco, E., 2008. Satellite observation of biomass burning: Implications in global change Research, *Earth Observation and Global Change* (E. Chuvieco, editor), Springer, New York, pp. 109–142.

Chuvieco, E., S. Opazo, W. Sione, H. Del Valle, J. Anaya, C. Di Bella, I. Cruz, L. Manzo, G. Lopez, N. Mari, F. Gonzalez, F. Morelli, A. Setzer, I. Csiszar, A. Karpandegui, A. Bastarrika, and R. Libonari, 2008. Global burned land estimation in Latin America using MODIS composite data, *Ecological Applications*, 18(1):64–79.

Fassnacht, K., W. Cohen, and T.A. Spies, 2006. Key issues in making and using satellite-based maps in ecology: A primer, *Forest Ecology and Management*, 222:167–181.

Fearnside, P.M., 2000a. Global warming and tropical land-use change: Greenhouse gas emissions from biomass burning, decomposition and soils in forest conversion, shifting cultivation and secondary vegetation, *Climate Change*, 46:115–158.

Fearnside, P.M., 2000b. Global warming and tropical land-use change: Greenhouse gas emissions from biomass burning, decomposition and soils in forest conversion, shifting cultivation and secondary vegetation, *Climatic Change*, 46:115–158.

Giglio, L., T. Loboda, D.P. Roy, B. Quayle, and C.O. Justice, 2009. An active-fire based burned area mapping algorithm for the MODIS sensor, *Remote Sensing of Environment*, 113(2):408–420.

Hoelzemann, J.J., M.G. Schultz, G.P. Brasseur, and C. Granier, 2004. Global Wildland Fire Emission Model (GWEM): Evaluating the use of global area burnt satellite data, *Journal of Geophysical Research,* 109(D14S04):doi:10.1029/2003JD003666.

Hudson, W.D., and C.W. Ramn, 1987. Correct formulation of the kappa coefficient of agreement, *Photogrammetric Engineering & Remote Sensing*, 53(4):421–422.

Levine, J.S., 2000. Global biomass burning: A case study of the gaseous and particulate emissions released to the atmosphere during the 1997 fires in Kalimantan and Sumatra, Indonesia, *Biomass Burning and its Inter-relationships with the Climate System* (J.L. Innes, M. Beniston, and M.M. Verstraete, editors), Kluwer Academic Publishers, Dordrecht, Boston, London, pp. 15–31.

Levine, J.S., T. Bobbe, N. Ray, and R.G. Witt, 1999. Wildland fires and the environment: A global synthesis, *UNEP/DEIAEW/TR. 99-1*, pp. 1–52.

Miettinen, J., 2007. *Burnt Area Mapping in Insular Southeast Asia Using Medium Resolution Satellite Imagery*, University of Helsinki, Helsinki.

Miller, J.D., and S.R. Yool, 2002. Mapping forest post-fire canopy consumption in several overstory types using multi-tempora Landsat TM and ETM data, *Remote Sensing of Environment,* 82:481–496.

Romero-Ruiz, M., A. Etter, A. Sarmiento, and K. Tansey, 2010. Spatial and temporal variability of fires in relation to ecosystems, land tenure and rainfall in savannas of northern South America, *Global Change Biology*, 16:2013–2023.

Roy, D., P. Frost, C. Justice, T. Landmann, J. Roux, K. Gumbo, S. Makungwa, K. Dunham, R. Du Toit, K. Mhwandagara, A. Zacarias, B. Tacheba, O. Dube, J. Pereira, P. Mushove, J. Morisette, S. Santhana, and D. Davies, 2005a. The southern Africa fire network (SAFNet) regional burned area product validation protocol, *International Journal of Remote Sensing,* 26:4265–4292.

Roy, D., and T. Landmann, 2005. Characterizing the surface heterogeneity of fire effects using multi-temporal reflective wavelength data, *International Journal of Remote Sensing*, 26(19):4179–4218.

Roy, D.P., and L. Boschetti, 2009a. Southern Africa validation of the MODIS, L3JRC and GlobCarbon burned-area products, *IEEE Transactions on Geoscience and Remote Sensing,* 47:DOI 10.1109/TGRS.2008.2009000.

Roy, D.P., and L. Boschetti, 2009b. Southern Africa validation of the MODIS, L3JRC and GlobCarbon Burned-Area Products, *IEEE Transactions on Geoscience and Remote Sensing*, 47(4):1–13.

Roy , D.P., P.G.H. Frost, C. Justice , T. Landmann, J. Le Roux, K. Gumbo, S. Makungwa, K. Dunham, R. Du Toit, K. Mhwandagara, A. Zacarias, B. Tacheba, O.P. Dube, J.M.C. Pereira, P. Mushove, J.T. Morisette, S.K. Santhana Vannan, and D. Davies, 2005. The southern Africa fire network (SAFNet) regional burned-area product-validation protocol, *International Journal of Remote Sensing*, 26(19):4265–4292.

Roy, D.P., Y. Jin, P.E. Lewis, and C.O. Justice, 2005b. Prototyping a global algorithm for systematic fire-affected area mapping using MODIS time series data, *Remote Sensing of Environment*, 97(2):137–162.

Schultz, M.G., A. Heil, J.J. Hoelzemann, A. Spessa, K. Thonicke, J.G. Goldammer, A.C. Held, J.M. C. Pereira, and M. van het Bolscher, 2008. Global wildland fire emissions from 1960 to 2000, *Global Biogeochemical Cycles,* 22(GB2002):doi:10.1029/2007GB003031.

Seiler, W., and P.J. Crutzen, 1980. Estimates of gross and net fluxes of carbon between the biosphere and the atmosphere from biomass burning, *Climate Change*, 2:207–247.

Shakesby, R.A., P.J. Wallbrink, S.H. Doerr, P.M. English, C.J. Chafer, G.S. Humphreys, W.H. Blake, and K.M. Tomkins, 2007. Distinctiveness of wildfire effects on soil erosion in south-east Australian eucalypt forests assessed in a global context, *Forest Ecology and Management,* 238(1-3):347–364.

Silva, J.M.N., A.C.L. Sá, and J.M.C. Pereira, 2005a. Comparison of burned area estimates derived from SPOT-VEGETATION and Landsat ETM+ data in Africa: Influence of spatial pattern and vegetation type, *Remote Sensing of Environment*, 96:188–201.

Silva, J.M.N., A.C.L. Sá, and J.M.C. Pereira, 2005b. Comparison of burned area estimates derived from SPOT-VEGETATION and Landsat ETM+ data in Africa: Influence of spatial pattern and vegetation type, *Remote Sensing of Environment,* 96(2): 188–201.

Simon, M., S. Plummer, F. Fierens, J.J. Hoelzemann, and O. Arino, 2004. Burnt area detection at global scale using ATSR-2: The GLOBSCAR products and their qualification, *Journal of Geophysical Research*, 109(D14S02):doi:10.1029/2003JD003622.

Smith, J.H., S.V. Stehman, J.D. Wickham, and L. Yang, 2003. Effects of landscape characteristics on land-cover class accuracy, *Remote Sensing of Environment,* 84(3):342–349.

Tansey, K., J.-M. Grégoire, J.M. C. Pereira, P.Defourny, R. Leigh, J.-F. Pekel, A. Barros, J.N. M. Silva, E. van Bogaert, E. Bartholomé, and S. Bontemps, 2007. L3JRC - A global, multi-year (2000-2007) burnt area product (1 km resolution and daily time steps), *Proceedings of the Remote Sensing and Photogrammetry Society Annual Conference 2007*, Newcastle upon Tyne, UK.

Tansey, K., J.M. Gregoire, E. Binaghi, L. Boschetti, P.A. Brivio, D. Ershov, S.P. Flasse, R. Fraser, D. Graetz, M. Maggi, P. Peduzzi, J.M.C. Pereira, J.N.M. Silva, A. Sousa, and D. Stroppiana, 2004. A global inventory of burned areas at 1 km resolution for the year 2000 derived from SPOT Vegetation Data, *Climatic Change*, 67:345–377.

Ward, D., W.M. Hao, R.A. Susott, and R.E. Babbitt, 1996. Effect of fuel composition on combustion efficiency and emission factors for African savanna ecosystems, *Journal of Geophysical Research*, 101(d19):23,569–523, 576.

(Received 30 August 2010; accepted 23 May 2011; final version 21 June 2011)